Teijeira, Alvaro; Garasa, Saray; Luri-Rey, Carlos; de Andrea, Carlos; Gato, Maria; Molina, Carmen; Kaisho, Tsuneyasu; Cirella, Assunta; Azpilikueta, Arantza; Wculek, Stefanie K; Egea, Josune; Olivera, Irene; Rodriguez, Inmaculada; Rouzaut, Ana; Verkhusha, Vladislav; Valencia, Karmele; Sancho, David; Berraondo, Pedro; Melero, Ignacio. Depletion of conventional type-1 dendritic cells in established tumors suppresses immunotherapy efficacy. Cancer research. 2022 Sep 21 ISSN 1538-7445 doi: 10.1158/0008-5472.CAN-22-1046

Depletion of conventional type-1 dendritic cells in established tumors suppresses immunotherapy efficacy

Short Title: cDC1 depletion hinders cancer immunotherapy.

Alvaro Teijeira[1,2,3], Saray Garasa[1,2], Carlos Luri-Rey[1], Carlos de Andrea[2,4], Maria Gato[1], Carmen Molina[1], Tsuneyasu Kaisho[5], Assunta Cirella[1], Arantza Azpilikueta[1,2,3], Steffanie K. Wculek[6], Josune Egea[1], Irene Olivera[1], Inmaculada Rodriguez[1,2,3], Ana Rouzaut[1,2], Vladislav Verkusha[7], Karmele Valencia[2,3,8], David Sancho[6], Pedro Berraondo[1,2,3], Ignacio Melero[1,2,3,9].

[1]Immunology and Immunotherapy department. CIMA, Universidad de Navarra. Pamplona, Spain.

[2]Navarra Institute of health research (IDISNA). Pamplona, Spain.

[3] Centro de Investigación Biomédica en Red en Oncología (CIBERONC). Madrid, Spain.

[4]Pathology department. Clinica Universidad de Navarra. Pamplona, Spain.

[5]Department of Immunology, Institute of Advanced Medicine, Wakayama Medical University, Wakayama, Japan.

[6] Immunobiology Lab. Centro Nacional de Investigación Cardiovasculares (CNIC). Madrid, Spain.

[7]Department of Anatomy and Structural Biology, Albert Einstein College of Medicine, Bronx, NY 10461, USA;

[8]Oncology department. CIMA, Universidad de Navarra. Pamplona, Spain.

[9]Deparments of Immunology and Oncology. Clinica Universidad de Navarra.

Correspondence to: Alvaro Teijeira or Ignacio Melero; ateijeiras@unav.es, imelero@unav.es. Immunology and Immunotherapy department, CIMA, Universidad de Navarra. Avda Pio XII, 55. 31008, Pamplona, Spain.

Conficts of interest: I.M. reports advisory roles with Roche-Genentech, Bristol-Myers Squibb, CYTOMX, Incyte, MedImmune, Tusk, F-Star, Genmab, Molecular Partners, Alligator, Bioncotech, MSD, Merck Serono, Boehringer Ingelheim, Astra Zeneca, Numab, Catalym, Amunix and Hotspot, and research funding from Roche, BMS, AstraZeneca, Genmab, Alligator, and Bioncotech. P.B. reports advisory roles with Tusk and Moderna, research funding from Sanofi, and Bavarian Nordic and

speaker honoraria from BMS, MSD, Novartis and AstraZeneca. The other authors declare that they have no competing interests.

Word Count. 5,005

Number of figures. 7

References. 56

ACKOWLEDGEMENTS.

This work was supported by Spanish Ministry of Economy and Competitiveness and Spanish Ministry of Research (MINECO SAF2014-52361-R and SAF 2017-83267-C2-1R and PID2020-112892RB-100, PID2020-113174-RA-100 [AEI/FEDER,UE], financed by MCIN/AEI/10.13039/501100011033), Cancer Research Institute under the CRI-CLIP, Asociación Española Contra el Cancer (AECC) Foundation under Grant GCB15152947MELE, Joint Translational Call for Proposals 2015 (JTC 2015) TRANSCAN-2 (code: TRS-2016-00000371), projects PI14/01686, PI13/00207, PI16/00668, PI19/01128, funded by Instituto de Salud Carlos III and co-funded by European Union (ERDF, "A way to make Europe"), European Commission within the Horizon 2020 Programme (PROCROP - 635122), Gobierno de Navarra Proyecto LINTERNA Ref: 0011–1411, Mark Foundation, Fundación BBVA and Fundación Olga Torres. AT is supported by the Ramon y Cajal program from the Spanish Ministry of Science (RYC2019-026406-I financiada por MCIN/AEI /10.13039/501100011033 y por El FSE invierte en tu futuro).

Esther Guirado and Dr. Belen Palencia are acknowledged for project managing, Dr. Diego Alignani for excellent flow cytometry assistance, the light microscopy unit and Carlos Ortiz de Solórzano for their support in microscopy experiments and Dr. Paul Miller for English editing.

ABSTRACT

The ability of conventional type-1 dendritic cells (cDC1) to cross-present tumor antigens to CD8+ T cells is critical for the induction of antitumor cytotoxic T lymphocytes. Mice that are constitutively deficient in cDC1 cells have been reported to fail to respond to immunotherapy strategies based on checkpoint inhibitors. However, further work is needed to clarify the precise time during immunotherapy treatment that cDC1 cells are required for the beneficial effect of treatment. Here, we used a refined XCR1-DTR-Venus transgenic mouse model to acutely deplete cDC1 cells and trace their behavior using intravital microscopy. Diphtheria toxin-mediated cDC1 depletion prior to immunotherapy treatment with anti-PD-1 and/or anti-CD137 immunostimulatory monoclonal antibodies (mAbs) completely ablated anti-tumor efficacy. The efficacy of adoptive T-cell therapy was also hampered by prior cDC1 depletion. After the onset of immunotherapy treatment, depletion of cDC1s only moderately reduced the therapeutic efficacy of anti-PD-1 and anti-CD137 mAbs. Intravital microscopy of liver-engrafted tumors revealed changes in the intratumoral behavior of cDC1 cells in mice receiving immunotherapy, and treatment with diphtheria toxin to deplete cDC1s impaired tumor T-cell infiltration and function. These results reveal that the functional integrity of the cDC1 compartment is required at the onset of various immunotherapies to successfully treat established tumors.

STATEMENT OF SIGNIFICANCE

These findings reveal the intratumoral behavior of cDC1 dendritic cells in transgenic mouse models and demonstrate that the efficacy of immunotherapy regimens is precluded by elimination of these cells.

INTRODUCTION

Crosspriming is a key function that controls the induction of antigen-specific cytotoxic T lymphocytes. The ability to uptake cellular remains and process the engulfed antigens for MHC class I presentation was discovered to be mainly performed by a minority subset of dendritic cells (DCs) (1). Such myeloid dendritic cells are known as conventional-type 1 dendritic cells (cDC1) (2). They were first identified in the spleen of mice as the $CD11c^+$ $DEC205^+$ $CD8\alpha^+$ whose involvement in CD8 T-cell responses was shown (3-5).

Detailed study of the transcripts and proteins expressed by dendritic cells better profiled this crosspresenting subset, that is characterized by the surface co-expression of CD11c, XCR1 and DNGR-1 (2). In mice, two subsets of cDC1 cells have been identified depending on expression of the CD103 integrin, which defines the $CD103^+$ migratory cDC1s and a $CD103^-$ resident subtype constitutively located in secondary lymphoid organs (6).

Much of the research pertaining to cDC1 function comes from the fact that this subset of DC needs the transcription factors BATF3 and IRF8 for their ontogeny in the bone marrow (7). Hence, *Batf3* knock out mice are selectively devoid of cDC1 cells (8,9). Interestingly, *Batf3*$^{-/-}$ mice are severely deficient when it comes to mounting anti-viral CTL responses as well as rejecting immunogenic spontaneously regressing tumor cell lines (8). Similarly, other mouse strains lacking cDC1 cells (e.g. XCR-1 DTA mice) show impaired anti-tumor immune responses (10). The main mechanisms carried out by cDC1 cells are MHC class I presentation of exogenous antigens (crosspresentation) and responsiveness to viral double stranded RNA (dsRNA) via endosomal TLR3 (11), giving rise to high levels of interleukin 12 production (12). The function of these dendritic cells is critically upregulated by type-I interferons (13,14) and activated helper CD4 T cells expressing CD40L (13). The exact molecular mechanism that redirects endosomal engulfed material to MHC I for antigen presentation is as yet incompletely understood, although there is genetic evidence for the involvement of proteins related to vesicular trafficking such as WDFY4 (15) and Sec22b (16).

Two groups simultaneously reported that tumor immunotherapy with anti-PD-1 and anti-CD137 mAbs was ineffective in cDC1-deficient *Batf3*$^{-/-}$ mice (17,18). The mechanisms could be traced to dysfunctional crosspriming of surrogate tumor antigens (18). Interestingly, adoptive T-cell therapy is also less efficient in *Batf3* knock-out mice showing a complete lack of antigen spreading that was needed to prevent tumor relapse (19-21). IL-12 production by cDC1 cells has also been shown to play a key role in PD-1 blockade anti-tumor efficacy (22).

In humans, cDC1 cells can be identified since they share with their mouse counterparts the expression of XCR1 and DNGR1 (23-25). In peripheral blood, they are best identified by the co-expression of CD141 (BDCA3) (26). Numbers of cDC1 cells in mice and humans are greatly increased by treatment with a soluble form of Flt3L which promotes their ontogeny in the bone marrow (27-29).

The involvement of cDC1 cells in cancer immunology and immunotherapy was underscored by observations according to which, tumors failing to produce the CCL4 or CCL5 chemokines that attract cDC1 cells behave as poorly immunogenic (30,31). In human tumors, a transcriptional cDC1 signature and the expression of *Batf3* are strongly associated with the levels of $CD8^+$ T cell infiltration (32-34). Reportedly, migratory cDC1s take up tumor antigen in mouse models (35) and may transfer it to secondary lymphoid organ-resident cDC1 cells (36). cDC1 cells seem to have a close functional interaction with NK cells (32,37), which is counter regulated by prostaglandins (38).

One important question that remains unanswered is whether cDC1 cells are required once immunotherapy has been instigated to mediate and sustain the beneficial effect of treatment. With the help of XCR1-DTR-Venus transgenic mice (39), we have demonstrated that diphtheria toxin-mediated depletion of cDC1 cells upon treatment hampers response to various immunotherapy agents. Moreover, microscopy imaging indicates that cDC1 cells actively interact with tumor antigen-specific T cells in the tumor microenvironment and are involved in tumor T-cell infiltration.

MATERIAL AND METHODS

Mice and cell lines

Mice were housed at the animal facility of the CIMA Universidad de Navarra (Pamplona, Spain). XCR1-DTR-VENUS (Xcr1$^{tm2(HBEGF/Venus)Ksho}$) mice were obtained from the RIKEN bioresource research center and have been described elsewhere (39). Mice were bred homozygous and crossed with C57BL/6 mice (Envigo, Barcelona) to obtain F1 heterozygous XCR1-DTR-Venus mice . hCD2RFP (C57BL/6 hCD2-DsRed) transgenic mice were a kind gift from Mark Coles from University of York (40) and were bred to OT-I mice (Jackson, C57BL/6-Tg(TcraTcrb)1100Mjb/J, RRID:IMSR_JAX:003831) to obtain F1 hCD2RFPxOT-I mice. *Batf3*$^{-/-}$ mice (B6.129S(C)-Batf3$^{tm1Kmm/J}$, RRID:IMSR_JAX:013755) were kindly provided by Kenneth M Murphy (Washington University, St. Louis, MO)(8). OTI and CD45.1 (Jackson) were bred to homocygosity to allow in vivo cell tracking. All animal procedures were approved by the institutional animal experimentation ethics committee and the regional government of Navarra (protocol 036-18, 089-18 and 087-21). Ages of mice included in experiments ranged from 8 to 12 weeks.

B16-OVA mouse melanoma cells and MC38 mouse colon carcinoma cell lines were kindly gifted by Dr Lieping Chen (Yale University, New Haven, Connecticut, USA) and Dr Karl E Hellström (University of Washington, Seattle, Washington, USA), respectively. E0771 tumor cells were obtained from ATCC. B16.OVAiRFP670 tumor cells were generated by lipofectamine 2000 (Thermo Fisher) transfection of B16OVA cells with piRFP670-N1 (a gift from Vladislav Verkhusha; Addgene plasmid #45457; http://n2t.net/addgene:45457; RRID:Addgene_45457)(41) an expression plasmid and selected based on FACS sorting in a MoFloAstrios EQ cell sorter (Beckman Coulter). Cultures were tested for Myoplasm monthly using the Mycoalert kiet (Promega). These cell lines were authenticated by Idexx Radil (Case 6592-2012). Cell lines were subjected to two or three passages before using in the experiments. Activated OT-I cells for therapy and imaging experiments were prepared as previously described (20). Briefly, total splenocytes of OT-I or OT-I x hCD2^{RFP} mice were cultured at 10^6 cells/ml with 100ng/ml of SIINFEKL peptide and 30 U/ml of hIL-2 (Proleukin, Novartis) for 48 hours, then the medium was removed and cells were cultured at the same cell density for an additional 48 hours with 30 U/ml hIL-2 in the absence of SIINFEKL peptide. All cells were grown in Roswell Park Memorial Institute 1640 media supplemented with GlutaMAX (Gibco), 10% heat-inactivated fetal bovine serum

(FBS), 50 μ of M 2-mercaptoethanol, 100 U/mL of penicillin, and 100 μg/mL of streptomycin at 37°C with 5% CO_2 (complete media).

Mouse tumor studies

5×10^5 MC38, B16.OVA or E0771 tumor cells were subcutaneously injected into the right flank of XCR1-DTR-Venus or *Batf3*$^{-/-}$ mice. Mice were treated at the indicated time points with diphtheria toxin (Sigma) with a single i.p. dose of 1 μg/ml plus two additional doses of 0.5 μg/ml every three days to maintain full cDC1 depletion (when indicated in the figures). Tumors were measured every three days with a caliper and the volume was calculated (length × width^2/2). Additionally, mice were monitored for survival and euthanized when any tumor size reached a diameter of 15 mm or mice showed signs of distress. In some experiments, C57BL/6 mice deficient for BAFT3 were used. Mice were treated on the indicated days with 200 μg of anti-PD-1 (clone RPM1-14, Bio X cell, RRID:AB_1107747), anti-CD137 (clone 3H3, Bio X cell, RRID:AB_2687721), anti-CTLA4 (9D9, Bio X cell, RRID:AB_10949609) and Rat IgG control (Bio X cell, RRID:AB_2687813) when used in single treatment or with 100 μg/ml of each antibody when used in combination with other immunostimulatory antibodies. For adoptive transfer experiments, mice were i.v. injected with $2x10^6$ activated OT-I cells that were isolated and cultured as explained above.

Flow cytometry

For the analysis of cDC1 depletion of XCR1-DTR-Venus in tumors, draining lymph nodes (dLN) and spleen, MC38-bearing mice were treated with a single dose of 1μg of DT and were sacrificed at the indicated time points. For the analysis of CD8 T cells, mice were injected with $0.5x10^6$ B16OVA cells. At day 6, mice were treated with 1 μg of DT, at day 7 mice were transferred with $2x10^6$ activated OTI CD8$^+$ T cells and at days 9 and 12 mice were treated with additional 0.5 μg of DT. Mice were treated with anti PD-1 and anti CD137 antibodies at day 10 and tumors and TDLN were harvested at day 14 after tumor inoculation. In the MC38 model, DT was injected at days 6 and 9 and antibodies at day 7 and 10 after tumor cell injection. Tumors and TDLN from euthanized mice were harvested at day 11. Organs were collected and single-cell suspensions were stained with the following antibodies: CD8α (BV510 ,RRID:AB_2561389; APC, RRID:AB_312750; BUV395, RRID:AB_2732919), F4/80 (PeCy7,

RRID:AB_893490; BV421, RRID:AB_10901171), TCRβ BV605 (RRID:AB_2687544), CXCR6 PeCy7 (RRID:AB_2721669), PD-1 PercpCy5.5 (RRID:AB_10550092), Tox PE (RRID:AB_10853657), Ki67 AF488 (RRID:AB_10900418), TCF7 AF647 (RRID:AB_2797631), CD11c (APC, RRID:AB_313778; BV510, RRID:AB_2562010), IA/IE (APC Fluor 780, RRID:AB_1548783; Percp-Cy5.5, RRID:AB_2191072), CD103 PE (RRID:AB_535948), CD11b (BUV395, RRID:AB_2740936; PeCy7, RRID:AB_312798),CD45.2 (PB, RRID:AB_492873; BUV496, RRID:AB_2870691) CD45.1 BV786 (RRID:AB_2740538) (all from Biolegend or BD, except TCF7 that was from Cell Signaling and Tox from BD)(42). Immunostained cells were analyzed with a Cytoflex LX or XS (Beckmann Coulter) or a FACsCANTO flow cytometer (BD). Fluorescence minus one or biological comparison controls were used for cell analysis. FlowJo software (TreeStar) was used for data analysis.

Multiplexed immunofluorescence staining

A six-color multiplex immunofluorescence panel based on tyramide signal amplification was used for simultaneous detection of CD3 (T cells, RRID:AB_443425), CD8 (cytotoxic T lymphocytes (CTLs), RRID:AB_2756376), Foxp3 (regulatory T cells, RRID:AB_2797979), CD4 (T helper cells, RRID:AB_2798898), CD11b (myeloid cells, RRID:AB_1216361) and Ki67 (proliferating cells, RRID:AB_443209) and diamidino-2-phenylindole (DAPI) on tumor sections from formalin-fixed paraffin-embedded (FFPE) samples as previously described (43). Briefly, 4 μm thick sections obtained from FFPE tissue blocks were deparaffinized and rehydrated from ethanol to water. Antigen retrieval with citrate (pH6, PerkinElmer) or EDTA (pH9, Dako) target retrieval solution was performed at the beginning of each sequential round of antibody staining. Each round consisted of heat-induced antigen retrieval followed by protein blocking (Antibody Diluent/Block, Akoya Bioscience), incubation with primary antibody, anti-rabbit secondary antibody (Opal Polymer anti-rabbit horseradish peroxidase Kit, Perkin Elmer) finishing with Opal fluorophore incubation diluted in 1XPlus Amplification Diluent (Akoya Bioscience). The panel primary antibody description is provided in supplementary materials. and sections were mounted with Faramount Aqueous Mounting Medium (Dako).

Whole tissue sections were scanned on a Vectra-Polaris Automated Quantitative Pathology Imaging System (Akoya Biosciences). Akoya Biosciences' Inform software (V.2.4.8) was used to remove the autofluorescence as determined by an unstained slide and to perform the spectral unmixing of the images. To analyze the invasive margin six rectangular regions were randomly

selected for each tumor containing the tumor margins, analyzed and the mean infiltration denoted by each marker for each tumor section was plotted.

Intravital Microscopy experiments

For intravital microscopy of B16OVA tumors engrafted in the liver, the spleens of XCR1-DTR-Venus mice were surgically exposed under isoflurane anesthesia and 10^6 B16.OVA.iRFP670 cells were injected in 50µl of PBS. Then, spleens were surgically removed, and mice were allowed to recover. Four days later mice were i.v. injected with activated 5 x 10^6 OTIxhCD2^{RFP} CTLs. Mice were i.p. injected with anti-PD-1 plus anti-CD137 or Rat IgG control mAbs at day 7 or 9 after tumor cell injection and DT was given 24 hours before such Ab treatments as indicated in the figures. At day 9, 11 after tumor cell injection, intravital confocal microscopy of the liver was performed as previously described (44,45). Mice were injected with 5 µg of CD31-AF647 antibody (RRID:AB_2161030). Briefly, the liver was surgically exposed and isolated from respiratory movements by separating the rib cage by pulling with a thread and keeping the liver tissue adhered to the coverslip with the help of wet pieces of paper. The temperature of the mice was maintained with a rectal probe connected to a heating blanket (Kemp) and mice were kept asleep under Isoflurane anesthesia (2%). Mice were placed on a custom-built stage and imaged with an LSM880 inverted microscope (Zeiss) equipped with a 25X water immersion objective (NA, 0.8). Imaging sessions took from 2 to 4 hours per mice and time-lapse acquisitions lasted from 30 minutes to 2 hours with frames taken every two minutes. Several tumor foci were imaged per session and mice. Time-lapse videos were analyzed using the IMARIS (Bitplane) software. Both Venus-positive and RFP$^+$ cells were segmented using the spots tool and tracked manually overtime. Individual cell motility parameters were generated from such tracks. Speed (track length/time), chemotactic index or straightness (Track displacement length/track length) and motility index (track displacement length^2/4*track duration) were calculated. Interactions of T cells with Venus´-positive cells were quantified selecting time points in which Venus$^+$ cells were closer than 12 µm from an RFP$^+$ CD8$^+$ T cell.

Time-lapse videos were generated in IMARIS software and edited with Final Cut Pro (Apple software).

Quantification and statistical analysis

Data were processed using GraphPad Prism 6.0. Means and standard error of the means are presented as averages and error bars unless otherwise indicated in the figure legends. All experimental repetitions and numbers of specimens and mice are indicated in the figure legends. For the statistical comparison of tumor growth individual areas under the curves (AUC) were calculated for each mouse and compared using ANOVA tests, which were used to analyze statistical differences between independent groups unless otherwise indicated. p values are shown for any relevant statistical difference in the figures.

Data availability

The data generated in this study are available upon request from the corresponding authors.

RESULTS

Depletion of cDC1 cells in the tumor tissue microenvironment and tumor-draining lymph nodes in XCR1-DTR-Venus transgenic mice

To investigate the need for the presence of cDC1 cells during immunotherapy, we made use of XCR1-DTR-Venus transgenic mice (39). cDC1 cells can be identified upon flow cytometry analysis of $CD11c^+$ $CD11b^-$ cells because of selective expression of the Venus fluorescent protein. We engrafted MC38 derived tumors under the skin of XCR1-DTR-Venus mice and intraperitoneally injected diphtheria toxin (Fig 1A).

Twenty-four hours after DT treatment, splenic $CD11c^+$ $CD11b^-$ $CD8\alpha^+$ cells almost disappeared, a phenomenon that was also observed in terms of the disappearance of MHC-II^+ $Venus^+$ cells (Figs 1B-D, supplementary fig S1A). Tumor-draining lymph nodes experienced a similar outcome following DT treatment (Figs 1B-D, supplementary fig S1A). In excised tumors, all $Venus^+$ DCs and most $CD103^+$ $CD11c^+$ $MHCII^+$ $F4/80^-$ dendritic cells were absent as a result of DT treatment (Figs 1B-D, supplementary fig S1A). In contrast, cDC2s were respected upon DT treatment (Supplementary fig S1B). Depletion of cDC1 cells following a single DT injection lasted for at least 5 days (Supplementary fig S1C). cDC1 cell numbers remained low for five days and eventually recovered when mice were analyzed at day 7 post DT treatment (Supplementary fig S1D).

cDC1 cells are required for the successful treatment of established tumors with various immunotherapy agents

We used the MC38 tumor model to characterize the need for cDC1 cells during treatment with efficacious immunotherapies. MC38-derived subcutaneous tumors partially respond to anti-CD137, or to anti-PD-1 mAbs and intensely respond to a combination of anti-CD137 plus anti-PD-1 mAbs (18). Experiments of DT depletion and immunostimulatory mAb treatments were performed in MC38 tumor-bearing XCR1-DTR-Venus transgenic mice and in *Batf3* knockout mice (Fig 2A). DT treatment started at day 4 after tumor inoculation, while the first immunostimulatory mAb was given at day 5. At day 4 the expansion of anti gp70 tumor reactive CD8 T cells were readily detectable in such tumor-bearing mice (Supplementary fig S2A). The partial efficacy of treatment of anti-PD-1 or anti-CD137 mAbs was lost in the groups of mice pretreated with DT (Figure 2B). The synergistic

immunotherapy combination of anti-PD-1 plus anti-CD137 mAbs was very efficacious, eradicating 14 out of 20 tumors, and again such efficacy was completely lost in DT-treated mice and in cDC1 constitutively deficient *Batf3*$^{-/-}$ mice (Fig 2C). In sentry mice from the experiments in figure 2B and C, cDC1 cells were verified as having been efficiently depleted (Supplementary fig S2B). Of note, DT treatment did not impair the efficacy of immunotherapy in WT mice (Supplementary fig S2C).

To study when cDC1 cells were needed for immunotherapy efficacy, we performed DT-mediated depletion at different time points. Mice that recovered from pre-engraftment transient depletion attained similar efficacy upon anti-CD137 plus anti-PD-1 treatment (Fig 2D). However, tumor growth prior to immunotherapy onset was hastened in pre-depleted groups, suggesting an immunotherapy-independent cDC1-mediated control of tumor progression at least in this tumor model (Fig 2D). When DT treatment was performed 1 day after the first immunotherapeutic mAb injections (Fig 2E), anti-PD-1 and anti-CD137 efficacy were reduced upon cDC1 depletion but the efficacy of the combination of both antibodies was retained irrespective of cDC1 cell depletion at that timepoint.

In the clinic, anti-PD-1 plus anti-CTLA-4 (Nivolumab plus Ipilimumab) constitutes the approved treatment of choice in a number of malignancies (46-48). Figure 3A shows that treatment with a mouse surrogate of such a combination lost most of its efficacy upon DT treatment against the transplanted E0771 breast cancer model. Interestingly, when testing cDC1 depletion in anti-PD-1 and anti-CTLA-4 based immunotherapies, cDC1 cells were only required for the efficacy of PD-1 blockade but not for the efficacy of anti-CTLA-4 mAbs (Fig 3B).

Adoptive T-cell therapy is also gaining clinical application (49,50). To model it, we used B16.OVA engrafted tumors and adoptive transfer of activated OT-I TCR-transgenic T cells recognizing OVA. Results in figure 3C indicate that the control of tumors by adoptively transferred OT-I cells was partially lost upon cDC1 depletion. These results are consistent with previous observations in *Batf3*$^{-/-}$ tumor-bearing mice treated with adoptive T-cell therapy (19), but highlight the relevance of cDC1s specifically during the administration of T cells.

In all previous experiments we used homozygous XCR1-DTR-Venus knock-in mice, that happen to have a disrupted XCR1 locus due to the fact that depletions were more efficient in such DTR homozygous mice. However, this created a doubt as to the potential importance of XCR1 for the efficacy of immunotherapy. This was ruled out as shown in supplementary figure S3, since therapies with anti-CD137+anti-PD-1 (Supplementary fig S3A), anti-PD-1+anti-CTLA-4 (Supplementary fig S3B)

and OT-I adoptive T-cell transfer (Supplementary fig S3C) were as efficacious in homozygous as in heterozygous transgenic mice, which have a functional XCR1 gene in the latter case.

cDC1 depletion reduces T-cell infiltration into the tumor microenvironment under immunotherapy and alters CD8-T cell stemness and exhaustion in tumor and TDLNs.

Focusing on the efficacy of anti-PD-1+anti-CD137 antibodies, we used multiplex tissue immunofluorescence to study the lymphocyte infiltrates of MC38 tumors under therapy with and without cDC1 depletion.

As can be seen in figure 4A at two different magnifications, DT-depletion caused a dramatic reduction of T cells infiltrating the tumor on day six after treatment onset, when mice had received two doses of immunostimulatory mAbs. Interestingly, upon cDC1 depletion, T cells remained on the rim of the invasive tumor margins without penetrating to the center of the engrafted tumor nodules (Fig 4A). Quantitative analysis and statistical comparisons of the images are provided in figure 4B and C, showing that the observed effects regarding T cell density were less prominent at the tumor margins.

It has been recently reported that during chronic LCMV infection cDC1 are able to support $TCF1^+$ $CD8^+$ precursor cells (51). The absence of cDC1 cells during the use of PD-1 blockade in the viral model induces a loss of $CD8^+$ T cells with precursor features ($TCF1^+$) enforcing their excessive proliferation and leading faster to exhaustion. To test the functional effects of cDC1 absence during immunotherapy in the cancer model setting, we implanted B16OVA tumors in XCR-1 DTR mice and adoptively transferred activated OVA specific $CD8^+$ $CD45.1^+$ OTI T cells to such mice to henceforth be able to trace antigen specific CD8 T cell-responses (Fig 5A). cDC1 depletion did not have any impact on the proportion of transferred OTI T cells recovered from the tumor draining LNs at the evaluated time point (5 days after starting cDC1 depletion, 4 days after immunotherapy onset). However, the recovered OTI $CD8^+$ T cells showed markedly less TCF7 expression, particularly in the absence of cDC1 during immunotherapy and showed upregulated CXCR6 expression as recently described in the LCMV chronic infection model (Fig 5B) (51). Immunotherapy enhanced the overall number of proliferating OTI cells, but proliferating cells were $TCF1^{low}$, mainly when cDC1 cells were absent. This was in contrast with the non-depleted mice in which proliferating cells were mainly $TCF7^{hi}$ (Fig 5C). We also analyzed the endogenous $CD8^+$ $PD1^+$ cells in the TDLNs (Fig 5D) and observed very similar results regarding TCF7 expression reduction (Fig 5E) and higher ki67-denoted proliferation in such $TCF7^{low}$

$CD8^+$ T cells (Fig 5F). In the tumor compartment we confirmed the impaired infiltration of transferred (Fig 5G) as a result of cDC1 depletion. Moreover, we observed increased expression of the exhaustion marker TOX2 in the absence of cDC1 cells during immunotherapy in OTI $CD8^+$ tumor infiltrating lymphocytes (Fig 5H). However, in this intratumoral location the effects of cDC1 depletion on TCF7 and proliferation were not as evident as in the TDLNs (Figs 5 I and J). In the endogenous $CD8^+$ tumor infiltrating lymphocytes less tumor infiltration, less exhaustion marker expression levels and similar TCF7 levels were also observed (Figs 5 K-M).

To test if these changes in CD8 T cells were observable in another tumor model, we analyzed endogenous $CD8^+$ T cells infiltrating MC38 tumors and from TDLNs in the same experimental conditions. The effects observed in the TDLN of such mice (Supplementary figs S4A-C) were similar to the ones observed in B16OVA TDLNs, but even more clear, with almost complete loss of TCF7 expression upon cDC1 depletion. In MC38 tumors, infiltrating $CD8^+$ T cells showed similar changes following cDC1 depletion, that included upregulation of exhaustion markers, loss of TCF7 expression and enhanced proliferation of the $TCF7^{low}$ population (Supplementary figs S4D-F).

To further understand the effects of cDC1 to sustain already activated T cells, we transferred T cells from MC38-bearing mice previously cured with immunotherapy (anti PD-1+anti-CD137 treated) into $Batf3^{-/-}$ recipient mice having no cDC1 cells or control WT mice. Transferred T cells were able to more efficaciously control tumors in WT mice than in cDC1-deficient $Batf3^{-/-}$ mice (Supplementary fig S4G).

Intravital microscopy evidence for cDC1 sustainment of $CD8^+$ T-cell responses in the tumor microenvironment under immunotherapy

The selective expression of Venus in $XCR1^+$ cDC1 cells in XCR1-DTR-venus mice offered an opportunity for in vivo time-lapse confocal microscopy to trace their presence and behavior. We chose a model in which mice bear metastatic melanoma lesions in the liver (Fig 6A) to allow tumor visualization. In this setting, tumor cells are injected into the spleen to disseminate through the portal vein ten days before imaging. Of note, spleens are removed to avoid unwanted tumor cell-engraftment in this organ. Multiple tumor nodules appeared in the liver when a B16OVA melanoma variant transfected to express the fluorescent protein iRFP670 was intrasplenically injected. Hence, fluorescent tumor cells expressing the surrogate antigen OVA can be visualized. Moreover, XCR1-DTR-Venus mice are adoptively transferred with pre-activated TCR-transgenic OT-1 T cells that are

co-transgenic for RFP to simultaneously permit visualization and tracking of anti-OVA tumor specific $CD8^+$ T cells (Fig 6B). The liver central lobe can be surgically exposed and microscopy imaging can be performed for up to four or five hours. Figure 6B and movie S1 show that cDC1 cells (bright green), OT-I cells (red) and B16OVA melanoma cells (blue) can be co-visualized overtime in this experimental setting. OT-I cells were activated before adoptive transfer to bypass possible effects of cDC1 cells on priming in these experiments.

Focusing on cDC1 cells (Fig 6C), we were able to trace their behavior and their interactions with OT-I cells. As can be seen in figure 6C and movie S2, some cDC1 cells actively moved (termed migrating cells in fig 6C) and interacted with T cells (cell #2 in fig 6C). First, when these experiments were performed in mice receiving anti-PD-1 plus anti-CD137 mAbs, given 48 hours earlier, more cDC1 cells could be found in the metastatic foci (Fig 6D). We observed a non-statistically significant upregulation of CCL5 mRNA within MC38 tumors treated with immunotherapy but no major changes in other DC chemoattracting chemokines as XCL-1 or CCL4 were found (Supplementary fig S5A) Monitoring cDC1 behavior overtime, we detected that a fraction of cDC1 cells established more durable interactions with OT-I cells in mice receiving immunotherapy as compared to cDC1 cells in mice receiving IgG control antibodies (Figure 6E). However, the cDC1 cells also tended to move at higher speeds (Figure 6F) in a direction that seemed purposeful, since the directionality of migration was also significantly higher under immunotherapy with the immunostimulatory antibodies (Fig 6G). When such experiments were performed in the absence of OTI (Supplementary fig S5B), we observed a similar effect regarding enhanced speed of cDC1 cells upon immunotherapy treatment but without increased directional movement, therefore implying that adoptively transferred OTI cells may underlie enhanced DC activation in these experiments.

Next, we focused on T-cell behavior comparing conditions in which mice had been depleted of cDC1 cells 72 hours earlier with DT and/or given immunotherapy with anti-PD-1 plus anti-CD137 mAbs. Most importantly, under conditions of immunotherapy, OT-I cells readily infiltrated the tumor, but such an increase was impaired by DT-mediated depletion of cDC1 cells (Fig 7A and B and movie S3).

We analyzed the behavior of T cells under immunotherapy with and without cDC1 depletion. Previous results using anti-CD137 treatment had shown that OT-I cells upon such immunotherapy stayed focused on targets and showed less overall motility (52). In keeping with these previous findings, OT-I cells under anti-PD-1 plus anti-CD137 immunotherapy showed reduced speed and motility (distance away from the initial location) (Fig 7C and D) and were more focused on the tumor

target cells (Movie S3). Notably, this focusing effect was lost when cDC1 cells were depleted by DT. Interestingly, $CD8^+$ T cells showed no differences in speed or motility in the surrounding non-tumor liver tissue (Fig 7C and D).

Overall, this intravital microscopy experimentation indicates that cDC1 cells are not only important to mediate infiltration of T cells recognizing tumor antigens, but also are able to change the functional T-cell behavior in the tumor tissue microenvironment.

DISCUSSION

The requirement for cDC1 cells to be present and functional immediately before immunotherapy treatments with immunostimulatory monoclonal antibodies is clearly demonstrated here. We took advantage of XCR1-DTR-Venus transgenic mice, which had been used before to reveal the role of cDC1 cells in the crosspriming of listeria antigens as well as in LCMV chronic infection (39,51). Diphtheria toxin depletions in the tumor microenvironment and tumor-draining lymph nodes were almost complete and lasted for at least five days. Nonetheless, our DT dosing scheme was more frequent to ensure complete cDC1 absence. These results are compatible with the lack of efficacy of various immunotherapies in *Batf3*$^{-/-}$ mice (17,18,53) and make the point that the presence of cDC1 cells at the onset of treatment is a must for immunotherapy to be efficacious. Our experiments do not yet address whether migratory (CD103^{+}) or secondary lymphoid organ-resident (CD103^{-}) cDC1 cells are those which are necessary and it may well be the case that both dendritic cell subsets play key roles (36).

Our previous experiments in *Batf3*$^{-/-}$ mice had shown that these cells were critically needed for antigen-specific CD8 T-cell priming in tumor-bearing mice (18). Importantly, these cDC1 cells are also key to prime against antigen material derived from cytotoxicity as mediated by NK, CTL and CAR T cells (21,54). Therefore, a virtuous circle is postulated according to which the cytotoxic effects of immunotherapy provide more raw-material for tumor antigen crosspresentation by cDC1 cells. The common feature is that cDC1 cells are continuously needed for immunotherapy agents such as anti-PD-1, anti-CD137, intratumoral poly I:C (53), radio-immunotherapy (55) and adoptive T-cell therapy (19-21). These facts speak of the key importance of the functions mediated by cDC1 cells in oncoimmunology approaches, either with approved or with promising agents under clinical-trial development (56).

In keeping with previous observations (30), we observe that cDC1 cells are critical to allow intratumoral T-cell infiltration. Our multiplex immunofluorescence images and time-lapse confocal intravital imaging are conclusive in that regard. The underlying mechanisms remain under investigation and probably involve chemokine loops under the IL-12-IFNγ axis as previously reported (30,31). Observations following OTI CD8^{+} T-cell transfer are also in agreement with this conclusion. Furthermore, cDC1 seem to be necessary to avoid the expression of exhaustion markers and maintain the markers related to stemness and self-renewal in such TCR transgenic OTI cells (51).

Intravital imaging of tumor metastases nested in the liver permitted time-lapse imaging of the tumors and the surrounding non-tumor liver parenchyma. Three facts became clear in these intravital microsocopy experiments: (i) cDC1 cells change their behavior under immunotherapy conditions within the tumor microenvironment. (ii) $CD8^+$ T cells recognizing tumor antigens are attracted and stimulated by cDC1 cells in the baseline tumor microenvironment and more intensely once immunotherapy has been instigated. (iii) cDC1 cells are required for optimal dynamics and function of $CD8^+$ T cells within the tumor microenvironment during immunotherapy. The quantitative parameters of motility, number and duration of cellular interactions in the liver nested-tumors are indirect measurements that estimate profound functional changes, even if the molecular mechanisms in action are probably multiple and remain to be fully elucidated. Complex bidirectional functional consequences of cDC1 interactions with cognate T cells are likely to ultimately underlie the efficacy of immunotherapy treatments.

Given the absolute requirement for the presence of cDC1 cells for immunotherapy of established tumors to be efficacious, strategies that enhance their presence and activity in tumors make a great deal of sense in clinical translation. For instance sFLT3L (28,29) or local delivery of chemokines attracting cDC1s (42) are strong partner candidates to enhance efficacy of various immunotherapy approaches.

REFERENCES

1. Joffre OP, Segura E, Savina A, Amigorena S. Cross-presentation by dendritic cells. Nat Rev Immunol **2012**;12:557-69
2. Cabeza-Cabrerizo M, Cardoso A, Minutti CM, Pereira da Costa M, Reis e Sousa C. Dendritic Cells Revisited. Annu Rev Immunol **2021**;39:131-66
3. den Haan JM, Lehar SM, Bevan MJ. CD8(+) but not CD8(-) dendritic cells cross-prime cytotoxic T cells in vivo. J Exp Med **2000**;192:1685-96
4. Vremec D, Zorbas M, Scollay R, Saunders DJ, Ardavin CF, Wu L*, et al.* The surface phenotype of dendritic cells purified from mouse thymus and spleen: investigation of the CD8 expression by a subpopulation of dendritic cells. J Exp Med **1992**;176:47-58
5. Steinman RM. Decisions about dendritic cells: past, present, and future. Annu Rev Immunol **2012**;30:1-22
6. Edelson BT, Kc W, Juang R, Kohyama M, Benoit LA, Klekotka PA*, et al.* Peripheral CD103+ dendritic cells form a unified subset developmentally related to CD8alpha+ conventional dendritic cells. J Exp Med **2010**;207:823-36
7. Murphy TL, Grajales-Reyes GE, Wu X, Tussiwand R, Briseno CG, Iwata A*, et al.* Transcriptional Control of Dendritic Cell Development. Annu Rev Immunol **2016**;34:93-119
8. Hildner K, Edelson BT, Purtha WE, Diamond M, Matsushita H, Kohyama M*, et al.* Batf3 deficiency reveals a critical role for CD8alpha+ dendritic cells in cytotoxic T cell immunity. Science **2008**;322:1097-100
9. Ataide MA, Komander K, Knopper K, Peters AE, Wu H, Eickhoff S*, et al.* BATF3 programs CD8(+) T cell memory. Nat Immunol **2020**;21:1397-407
10. Mattiuz R, Brousse C, Ambrosini M, Cancel JC, Bessou G, Mussard J*, et al.* Type 1 conventional dendritic cells and interferons are required for spontaneous CD4(+) and CD8(+) T-cell protective responses to breast cancer. Clin Transl Immunology **2021**;10:e1305
11. Schulz O, Diebold SS, Chen M, Naslund TI, Nolte MA, Alexopoulou L*, et al.* Toll-like receptor 3 promotes cross-priming to virus-infected cells. Nature **2005**;433:887-92
12. Gautier G, Humbert M, Deauvieau F, Scuiller M, Hiscott J, Bates EE*, et al.* A type I interferon autocrine-paracrine loop is involved in Toll-like receptor-induced interleukin-12p70 secretion by dendritic cells. J Exp Med **2005**;201:1435-46
13. Snijders A, Kalinski P, Hilkens CM, Kapsenberg ML. High-level IL-12 production by human dendritic cells requires two signals. Int Immunol **1998**;10:1593-8
14. Le Bon A, Etchart N, Rossmann C, Ashton M, Hou S, Gewert D*, et al.* Cross-priming of CD8+ T cells stimulated by virus-induced type I interferon. Nat Immunol **2003**;4:1009-15
15. Theisen DJ, Davidson JTt, Briseno CG, Gargaro M, Lauron EJ, Wang Q*, et al.* WDFY4 is required for cross-presentation in response to viral and tumor antigens. Science **2018**;362:694-9
16. Cebrian I, Visentin G, Blanchard N, Jouve M, Bobard A, Moita C*, et al.* Sec22b regulates phagosomal maturation and antigen crosspresentation by dendritic cells. Cell **2011**;147:1355-68
17. Salmon H, Idoyaga J, Rahman A, Leboeuf M, Remark R, Jordan S*, et al.* Expansion and Activation of CD103(+) Dendritic Cell Progenitors at the Tumor Site Enhances Tumor Responses to Therapeutic PD-L1 and BRAF Inhibition. Immunity **2016**;44:924-38
18. Sanchez-Paulete AR, Cueto FJ, Martinez-Lopez M, Labiano S, Morales-Kastresana A, Rodriguez-Ruiz ME*, et al.* Cancer Immunotherapy with Immunomodulatory Anti-CD137 and

Anti-PD-1 Monoclonal Antibodies Requires BATF3-Dependent Dendritic Cells. Cancer Discov **2016**;6:71-9
19. Spranger S, Dai D, Horton B, Gajewski TF. Tumor-Residing Batf3 Dendritic Cells Are Required for Effector T Cell Trafficking and Adoptive T Cell Therapy. Cancer Cell **2017**;31:711-23 e4
20. Etxeberria I, Bolanos E, Quetglas JI, Gros A, Villanueva A, Palomero J*, et al.* Intratumor Adoptive Transfer of IL-12 mRNA Transiently Engineered Antitumor CD8(+) T Cells. Cancer Cell **2019**;36:613-29 e7
21. Conde E, Vercher E, Soria-Castellano M, Suarez-Olmos J, Mancheno U, Elizalde E*, et al.* Epitope spreading driven by the joint action of CART cells and pharmacological STING stimulation counteracts tumor escape via antigen-loss variants. J Immunother Cancer **2021**;9
22. Garris CS, Arlauckas SP, Kohler RH, Trefny MP, Garren S, Piot C*, et al.* Successful Anti-PD-1 Cancer Immunotherapy Requires T Cell-Dendritic Cell Crosstalk Involving the Cytokines IFN-gamma and IL-12. Immunity **2018**;49:1148-61 e7
23. Poulin LF, Reyal Y, Uronen-Hansson H, Schraml BU, Sancho D, Murphy KM*, et al.* DNGR-1 is a specific and universal marker of mouse and human Batf3-dependent dendritic cells in lymphoid and nonlymphoid tissues. Blood **2012**;119:6052-62
24. Bachem A, Guttler S, Hartung E, Ebstein F, Schaefer M, Tannert A*, et al.* Superior antigen cross-presentation and XCR1 expression define human CD11c+CD141+ cells as homologues of mouse CD8+ dendritic cells. J Exp Med **2010**;207:1273-81
25. Sancho D, Mourao-Sa D, Joffre OP, Schulz O, Rogers NC, Pennington DJ*, et al.* Tumor therapy in mice via antigen targeting to a novel, DC-restricted C-type lectin. J Clin Invest **2008**;118:2098-110
26. Poulin LF, Salio M, Griessinger E, Anjos-Afonso F, Craciun L, Chen JL*, et al.* Characterization of human DNGR-1+ BDCA3+ leukocytes as putative equivalents of mouse CD8alpha+ dendritic cells. J Exp Med **2010**;207:1261-71
27. Morse MA, Nair S, Fernandez-Casal M, Deng Y, St Peter M, Williams R*, et al.* Preoperative mobilization of circulating dendritic cells by Flt3 ligand administration to patients with metastatic colon cancer. J Clin Oncol **2000**;18:3883-93
28. Hammerich L, Marron TU, Upadhyay R, Svensson-Arvelund J, Dhainaut M, Hussein S*, et al.* Systemic clinical tumor regressions and potentiation of PD1 blockade with in situ vaccination. Nat Med **2019**;25:814-24
29. Breton G, Zheng S, Valieris R, Tojal da Silva I, Satija R, Nussenzweig MC. Human dendritic cells (DCs) are derived from distinct circulating precursors that are precommitted to become CD1c+ or CD141+ DCs. J Exp Med **2016**;213:2861-70
30. Spranger S, Bao R, Gajewski TF. Melanoma-intrinsic beta-catenin signalling prevents anti-tumour immunity. Nature **2015**;523:231-5
31. Ruiz de Galarreta M, Bresnahan E, Molina-Sanchez P, Lindblad KE, Maier B, Sia D*, et al.* beta-Catenin Activation Promotes Immune Escape and Resistance to Anti-PD-1 Therapy in Hepatocellular Carcinoma. Cancer Discov **2019**;9:1124-41
32. Barry KC, Hsu J, Broz ML, Cueto FJ, Binnewies M, Combes AJ*, et al.* A natural killer-dendritic cell axis defines checkpoint therapy-responsive tumor microenvironments. Nat Med **2018**;24:1178-91
33. Garris CS, Luke JJ. Dendritic Cells, the T-cell-inflamed Tumor Microenvironment, and Immunotherapy Treatment Response. Clin Cancer Res **2020**;26:3901-7
34. Spranger S, Luke JJ, Bao R, Zha Y, Hernandez KM, Li Y*, et al.* Density of immunogenic antigens does not explain the presence or absence of the T-cell-inflamed tumor microenvironment in melanoma. Proc Natl Acad Sci U S A **2016**;113:E7759-E68

35. Roberts EW, Broz ML, Binnewies M, Headley MB, Nelson AE, Wolf DM*, et al.* Critical Role for CD103(+)/CD141(+) Dendritic Cells Bearing CCR7 for Tumor Antigen Trafficking and Priming of T Cell Immunity in Melanoma. Cancer Cell **2016**;30:324-36
36. Ruhland MK, Roberts EW, Cai E, Mujal AM, Marchuk K, Beppler C*, et al.* Visualizing Synaptic Transfer of Tumor Antigens among Dendritic Cells. Cancer Cell **2020**;37:786-99 e5
37. Bottcher JP, Bonavita E, Chakravarty P, Blees H, Cabeza-Cabrerizo M, Sammicheli S*, et al.* NK Cells Stimulate Recruitment of cDC1 into the Tumor Microenvironment Promoting Cancer Immune Control. Cell **2018**;172:1022-37 e14
38. Bonavita E, Bromley CP, Jonsson G, Pelly VS, Sahoo S, Walwyn-Brown K*, et al.* Antagonistic Inflammatory Phenotypes Dictate Tumor Fate and Response to Immune Checkpoint Blockade. Immunity **2020**;53:1215-29 e8
39. Yamazaki C, Sugiyama M, Ohta T, Hemmi H, Hamada E, Sasaki I*, et al.* Critical roles of a dendritic cell subset expressing a chemokine receptor, XCR1. J Immunol **2013**;190:6071-82
40. Veiga-Fernandes H, Coles MC, Foster KE, Patel A, Williams A, Natarajan D*, et al.* Tyrosine kinase receptor RET is a key regulator of Peyer's patch organogenesis. Nature **2007**;446:547-51
41. Shcherbakova DM, Verkhusha VV. Near-infrared fluorescent proteins for multicolor in vivo imaging. Nat Methods **2013**;10:751-4
42. Sanchez-Paulete AR, Teijeira A, Quetglas JI, Rodriguez-Ruiz ME, Sanchez-Arraez A, Labiano S*, et al.* Intratumoral Immunotherapy with XCL1 and sFlt3L Encoded in Recombinant Semliki Forest Virus-Derived Vectors Fosters Dendritic Cell-Mediated T-cell Cross-Priming. Cancer Res **2018**;78:6643-54
43. Alvarez M, Molina C, De Andrea CE, Fernandez-Sendin M, Villalba M, Gonzalez-Gomariz J*, et al.* Intratumoral co-injection of the poly I:C-derivative BO-112 and a STING agonist synergize to achieve local and distant anti-tumor efficacy. J Immunother Cancer **2021**;9
44. Marques PE, Antunes MM, David BA, Pereira RV, Teixeira MM, Menezes GB. Imaging liver biology in vivo using conventional confocal microscopy. Nat Protoc **2015**;10:258-68
45. Teijeira A, Garasa S, Gato M, Alfaro C, Migueliz I, Cirella A*, et al.* CXCR1 and CXCR2 Chemokine Receptor Agonists Produced by Tumors Induce Neutrophil Extracellular Traps that Interfere with Immune Cytotoxicity. Immunity **2020**;52:856-71 e8
46. Larkin J, Chiarion-Sileni V, Gonzalez R, Grob JJ, Rutkowski P, Lao CD*, et al.* Five-Year Survival with Combined Nivolumab and Ipilimumab in Advanced Melanoma. N Engl J Med **2019**;381:1535-46
47. Motzer RJ, Tannir NM, McDermott DF, Aren Frontera O, Melichar B, Choueiri TK*, et al.* Nivolumab plus Ipilimumab versus Sunitinib in Advanced Renal-Cell Carcinoma. N Engl J Med **2018**;378:1277-90
48. Yau T, Kang YK, Kim TY, El-Khoueiry AB, Santoro A, Sangro B*, et al.* Efficacy and Safety of Nivolumab Plus Ipilimumab in Patients With Advanced Hepatocellular Carcinoma Previously Treated With Sorafenib: The CheckMate 040 Randomized Clinical Trial. JAMA Oncol **2020**;6:e204564
49. Morotti M, Albukhari A, Alsaadi A, Artibani M, Brenton JD, Curbishley SM*, et al.* Promises and challenges of adoptive T-cell therapies for solid tumours. Br J Cancer **2021**;124:1759-76
50. Yang JC, Rosenberg SA. Adoptive T-Cell Therapy for Cancer. Adv Immunol **2016**;130:279-94
51. Dahling S, Mansilla AM, Knopper K, Grafen A, Utzschneider DT, Ugur M*, et al.* Type 1 conventional dendritic cells maintain and guide the differentiation of precursors of exhausted T cells in distinct cellular niches. Immunity **2022**;55:656-70 e8

52. Weigelin B, Bolanos E, Teijeira A, Martinez-Forero I, Labiano S, Azpilikueta A*, et al.* Focusing and sustaining the antitumor CTL effector killer response by agonist anti-CD137 mAb. Proc Natl Acad Sci U S A **2015**;112:7551-6
53. Aznar MA, Planelles L, Perez-Olivares M, Molina C, Garasa S, Etxeberria I*, et al.* Immunotherapeutic effects of intratumoral nanoplexed poly I:C. J Immunother Cancer **2019**;7:116
54. Minute L, Teijeira A, Sanchez-Paulete AR, Ochoa MC, Alvarez M, Otano I*, et al.* Cellular cytotoxicity is a form of immunogenic cell death. J Immunother Cancer **2020**;8
55. Rodriguez-Ruiz ME, Rodriguez I, Garasa S, Barbes B, Solorzano JL, Perez-Gracia JL*, et al.* Abscopal Effects of Radiotherapy Are Enhanced by Combined Immunostimulatory mAbs and Are Dependent on CD8 T Cells and Crosspriming. Cancer Res **2016**;76:5994-6005
56. Etxeberria I, Glez-Vaz J, Teijeira A, Melero I. New emerging targets in cancer immunotherapy: CD137/4-1BB costimulatory axis. ESMO Open **2020**;4:e000733

FIGURE LEGENDS

Figure 1. XCR1-Venus-DTR transgenic mice permit tracing and depletion of cDC1 cells in lymphoid organs and engrafted tumor tissue. A) Schematic view of XCR1-DTR-Venus and a representative FACS dot-plot of cells in the spleen showing CD11c on the X axis and Venus fluorescent protein on the Y axis. A population of Venus-positive cells can be observed only in the $CD11c^+$ population. Representative microphotograph of fluorescent Venus-positive cells within tumors are shown to highlight that cDC1 can also be tracked by fluorescence microscopy. B) Representative flow cytometry dot-plots showing cDC1 depletion as the percentage of $Venus^+$ cells among dendritic cells ($CD45^+$,$F4/80^-$,$CD11c^+$,MHC II^+) or based on cDC1 surface phenotype in the spleen ($CD45^+$,$F4/80^-$,$CD11c^+$,MHC II^+, $CD8\alpha^+$, $CD11b^-$), lymph nodes ($CD45^+$,$F4/80^-$,$CD11c^+$,MHC II^+, $CD103\alpha^+$, $CD11b^-$) and in the leukocyte infiltrate of MC38-derived tumors ($CD45^+$,$F4/80^-$,$CD11c^+$,MHC II^+, $CD103\alpha^+$, $CD11b^-$) 24 hours after DT intraperitoneal injection. C and D) Summary data from experiments as in B (n= 4 mice). Each dot represents a single mouse.

Figure 2. Abrupt depletion of cDC1 dendritic cells during immunotherapy with immunostimulatory monoclonal antibodies impairs its efficacy. A) Schematic timeline of subcutaneous tumor growth experiments in XCR1-DTR-Venus mice treated with the indicated immunostimulatory antibodies and/or DT. B) Tumor size follow-up studies in XCR1-DTR-Venus mice depleted or not from cDC1 and treated with 200 μg of anti-PD-1, anti-CD137 or Rat IgG as a control. Mean ± SEM are shown, n=6 mice per group. C) Tumor size follow-up studies in XCR1-DTR-Venus mice or *Batf3*$^{-/-}$ mice depleted or not of cDC1 and treated with 100 μg of anti-PD-1 plus anti-CD137 or Rat IgG as a control. Mean ± SEM are shown. The proportions of cured mice per group are shown in the adjacent legends. D) Schematic timeline and tumor size follow-up studies in XCR1-DTR-Venus mice pre-depleted or not with intraperitoneal DT two days prior to MC38 tumor cell inoculation and treated with 100 μg of anti-PD-1 plus anti-CD137 or Rat IgG (as shown in the scheme). E) Schematic timeline and tumor size follow-up studies in XCR1-DTR-Venus mice depleted or not with intraperitoneal DT starting one day after immunotherapy treatment with 200 μg of anti-PD-1 or anti-CD137 mAbs or 100 μg of anti-PD-1 plus anti-CD137 or Rat IgG (as shown in the scheme). The proportions of cured mice per group are shown in the adjacent legend. Mean ± SEM are shown, n=5,6

mice per group. ANOVA tests of areas under the curves (AUC) were performed for statistical analyses; p values are shown for statistical comparisons.

Figure 3. cDC1 depletion impairs the efficacy of PD-1 blockade and adoptive T-cell therapy. A) Schematic timeline (upper), summary of tumor size follow-ups (left) and individual tumor growth of E0771 tumors (right) implanted in XCR1-DTR-Venus mice depleted or not of cDC1 cells and treated with 100 μg of anti-PD-1 plus anti-CTLA-4 or Rat IgG. Mean ± SEM are shown, n=6 mice per group. B) Experiments as in B but using 200 μg of anti-PD-1 or 200 μg of anti-CTLA-4 as single immunotherapy treatments. C) Schematic timeline (upper), summary of tumor size follow-ups (left) and individual tumor growth of B16OVA tumors (right) implanted in XCR1-DTR-Venus mice depleted or not of cDC1 cells and treated with 2 i.v. infusions of 2 x 10^6 activated OT-I cells indicated with black arrows. Mean ± SEM are shown, n=8-12 mice per group. ANOVA tests of areas under the curves (AUC) were performed for statistical analyses; p values are shown.

Figure 4. Depletion of cDC1 cells during immunotherapy with immunostimulatory mAbs reduces tumor infiltration by T cells. A) Representative multiplex immunofluorescence images of MC38 tumors treated with two doses of anti-PD-1 plus anti-CD137 ± DT (tumors were harvested on day 9 after tumor cell inoculation). Widefield views are shown on the left (Bars: 200 μm). Zoomed-in images of the areas indicated by white rectangles on the left panel are shown on the right images (Bars: 50 μm). Images are from a representative tumor section from each condition. B) Quantification of infiltrated immune cells in the MC38 tumors in images as in A. C) Quantification of T-cell infiltrates only in the tumor margins. n= 5 mice per group. Mann-Whitney U tests were performed for statistical analyses; p values are shown.

Figure 5. In the absence of cDC1 cells, antitumor CD8 T cells show reduced stemness and increased expression of exhaustion markers. Mice bearing subcutaneous B16OVA tumors were transferred with 2x10^6 pre-activated OTI T cells and were treated or not with DT and anti-PD-1 +anti-CD137 antibodies. Cell suspensions derived from tumors and TDLNs were then analyzed by flow cytometry. OTI cells were gated based in their CD45.1 expression and endogenous CD8 T cells were gated as CD45.2. Panels A-F show analyses performed in T cells from the tumor draining lymph nodes (TDLN) and panels G-M show analyses performed in tumor infiltrating $CD8^+$ T cells. n=6-7 mice per

group. In the Rat IgG DT group, some marker analyses could not be performed in samples from a single mouse due to the very low numbers of recovered OTI cells in the TDLN. Mann-Whitney U tests were performed for statistical analyses; p values are shown.

Figure 6. cDC1 dendritic cells infiltrate the tumor microenvironment and better perform their functions under anti-PD-1 plus anti-CD137 immunotherapy. A) Scheme showing the setup for intravital microscopy of melanoma lesions spread to the liver of XCR1-DTR-Venus mice transferred with anti-tumor OTI $CD8^+$ T cells. B) Representative image of a metastatic melanoma lesion in the liver showing B16.OVAiRFP670 tumor cells (blue), and infiltrating $Venus^+$ cDC1 cells (Intense green) and anti-OVA specific red-fluorescent OT-I cells (red). Images correspond to Movie S1. C) Representative snapshots of a time-lapse sequence of a tumor visualized as in A, focusing on the behavior of cDC1 $Venus^+$ cells in the tumor. The sequence shows DCs actively migrating (3 and 4) or not moving (1 and 2); interacting (1) or not (2) with intratumor OVA-specific OT-I CTLs. Individual tracks of moving cDC1 cells are overlaid as yellow lines. The sequence corresponds to movie S2. D) Representative images showing differential cDC1 infiltration in tumor lesions (circles) in Rat IgG- or anti-PD-1 + anti-CD137-treated mice following the experimental scheme shown in A and quantification of cDC1 density per tumor lesion. n=3-4 mice per condition and each dot represents an individual tumor lesion. (E, F, G) Single-cell cDC1 behavior was tracked in time-lapse videos such as movies S1 and S2. cDC1 interaction time with CTLs (E), speed (F) and meandering index (directionality) (G) are shown. n=3-4 mice per condition; 2-3 lesions per mice, each dot represents a single tracked cell. Mann-Whitney U tests were performed for statistical analyses; p values are shown.

Figure 7. Impact of DT-mediated depletion of cDC1 cells on the behavior of antitumor CD8 T cells upon immunotherapy treatment. A) Representative snapshots of liver tumor lesions imaged as in figure 5 showing individual tracks (30-minute follow-up) of antitumor specific OT-I cells (red) to highlight enhanced focus of CTLs interacting with tumor cells. Tumors of XCR1-DTR-Venus mice treated with control IgG or anti-PD-1 + anti-CD137 mAbs and treated or not with DT are shown. B) Anti-OVA specific $CD8^+$ T-cell density in tumor lesions in each of the three conditions. n=2-3 mice per condition. Dots represent individual tumor lesions. C, D) Single cell behavior of anti-tumor fluorescent OTI cells was tracked in time-lapse videos as those shown in movie S3. Speed (C) and Motility coefficient (D) are shown for T cells within the tumor lesions or in the surrounding liver tissue in XCR1-Venus mice treated with Rat IgG (control), anti-PD-1+anti-CD137 mAb $\pm$ DT depletion as indicated.

n=2-3 mice per condition (1-3 tumor lesions per mice). Dots represent single cells. ANOVA tests were performed for statistical analyses; p values are shown.

Figure 1

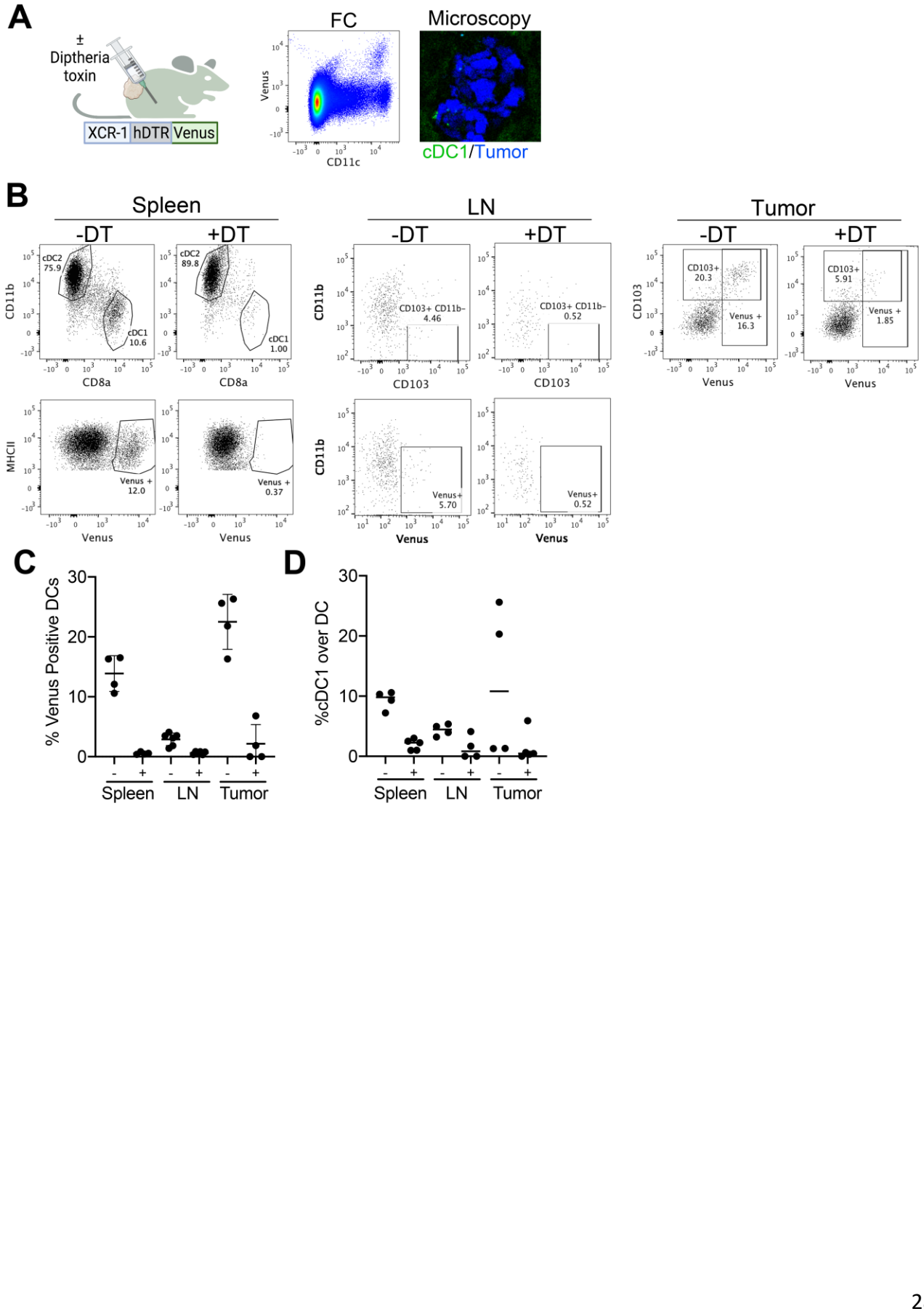
A
±
Diptheria
toxin
XCR-1 hDTR Venus
FC
Venus
CD11c
Microscopy
cDC1/Tumor
B
Spleen
LN
Tumor
-DT
+DT
CD11b
cDC2
75.9
cDC1
10.6
cDC2
89.8
cDC1
1.00
CD8a
CD103+ CD11b-
4.46
CD103+ CD11b-
0.52
CD103
CD103
CD103+
20.3
Venus +
16.3
CD103+
5.91
Venus +
1.85
Venus
MHCII
Venus +
12.0
Venus +
0.37
Venus+
5.70
Venus+
0.52
C
% Venus Positive DCs
D
%cDC1 over DC
Spleen
LN
Tumor

Figure 2

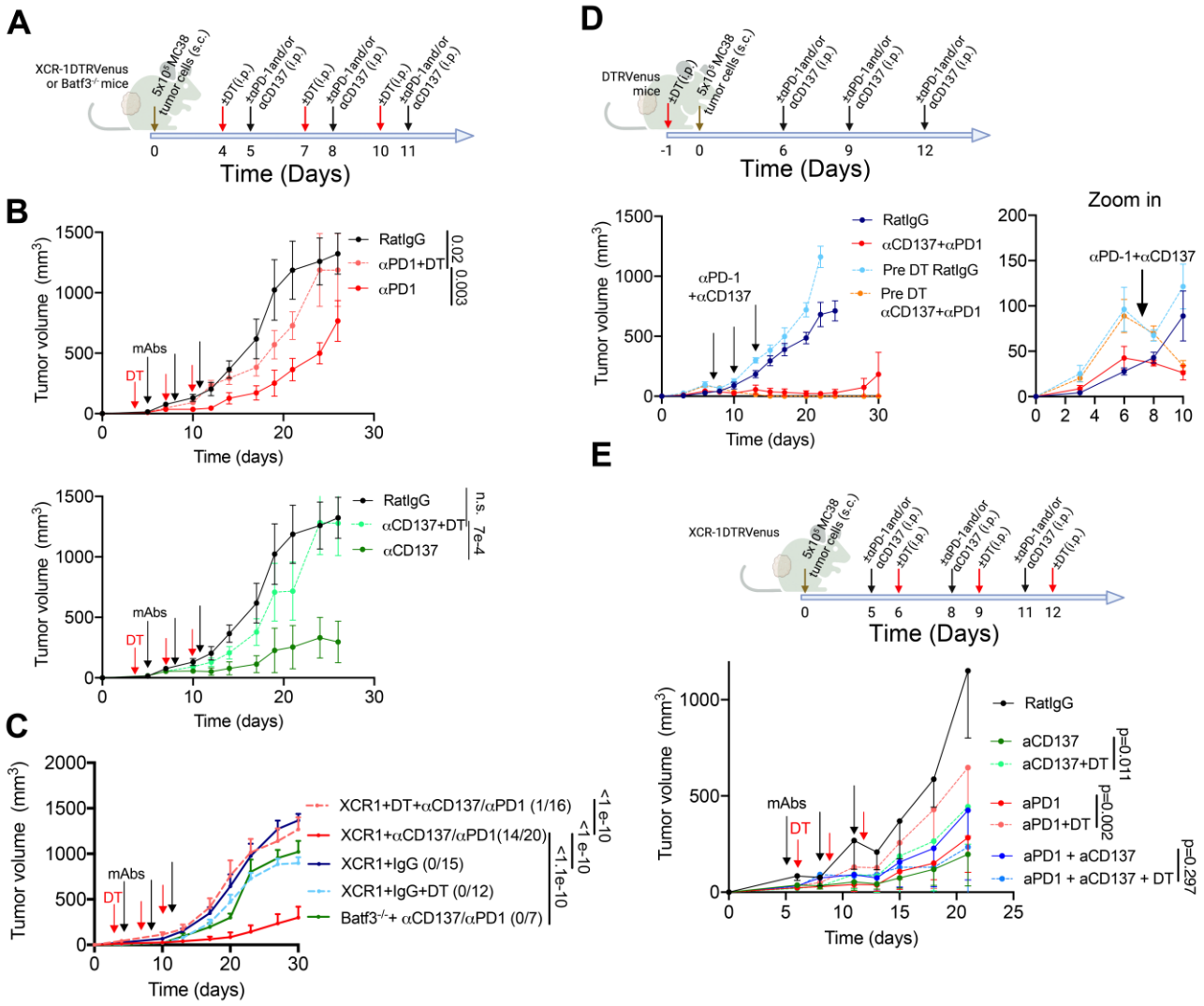
A
XCR-1DTRVenus or Batf3-/- mice
5x10^5 MC38 tumor cells (s.c.)
±DT(i.p.)
±αPD-1and/or αCD137 (i.p.)
0 4 5 7 8 10 11
Time (Days)
B
Tumor volume (mm3)
RatIgG
αPD1+DT
αPD1
0.02
0.003
mAbs
DT
Time (days)
RatIgG
αCD137+DT
αCD137
n.s.
7e-4
C
XCR1+DT+αCD137/αPD1 (1/16)
XCR1+αCD137/αPD1(14/20)
XCR1+IgG (0/15)
XCR1+IgG+DT (0/12)
Batf3-/-+ αCD137/αPD1 (0/7)
<1 e-10
<1 e-10
<1.1e-10
D
DTRVenus mice
-1 0 6 9 12
αPD-1 +αCD137
RatIgG
αCD137+αPD1
Pre DT RatIgG
Pre DT αCD137+αPD1
Zoom in
αPD-1+αCD137
E
XCR-1DTRVenus
0 5 6 8 9 11 12
RatIgG
aCD137
aCD137+DT
aPD1
aPD1+DT
aPD1 + aCD137
aPD1 + aCD137 + DT
p=0.011
p=0.002
p=0.297

Figure 3

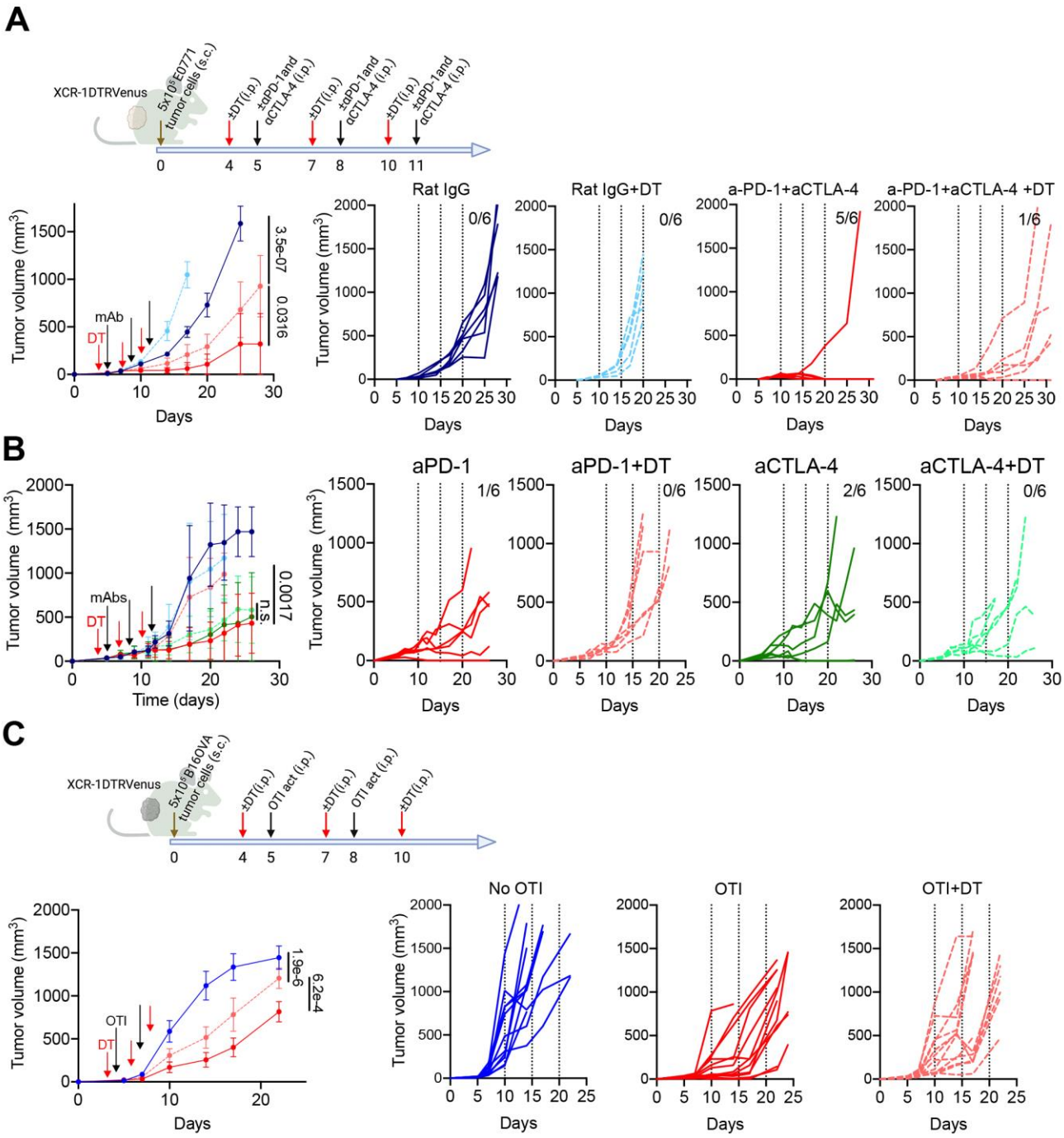
A
XCR-1DTRVenus
5x10⁵ E0771 tumor cells (s.c.)
±DT(i.p.)
±αPD-1and αCTLA-4 (i.p.)
0 4 5 7 8 10 11
Tumor volume (mm³)
mAb
DT
Days
3.5e-07
0.0316
Rat IgG
Rat IgG+DT
a-PD-1+aCTLA-4
a-PD-1+aCTLA-4 +DT
0/6
0/6
5/6
1/6
B
Time (days)
mAbs
0.0017
n.s.
aPD-1
aPD-1+DT
aCTLA-4
aCTLA-4+DT
1/6
0/6
2/6
0/6
C
XCR-1DTRVenus
5x10⁵ B16OVA tumor cells (s.c.)
±DT(i.p.)
OTI act (i.p.)
0 4 5 7 8 10
OTI
DT
1.9e-6
6.2e-4
No OTI
OTI
OTI+DT

Figure 4

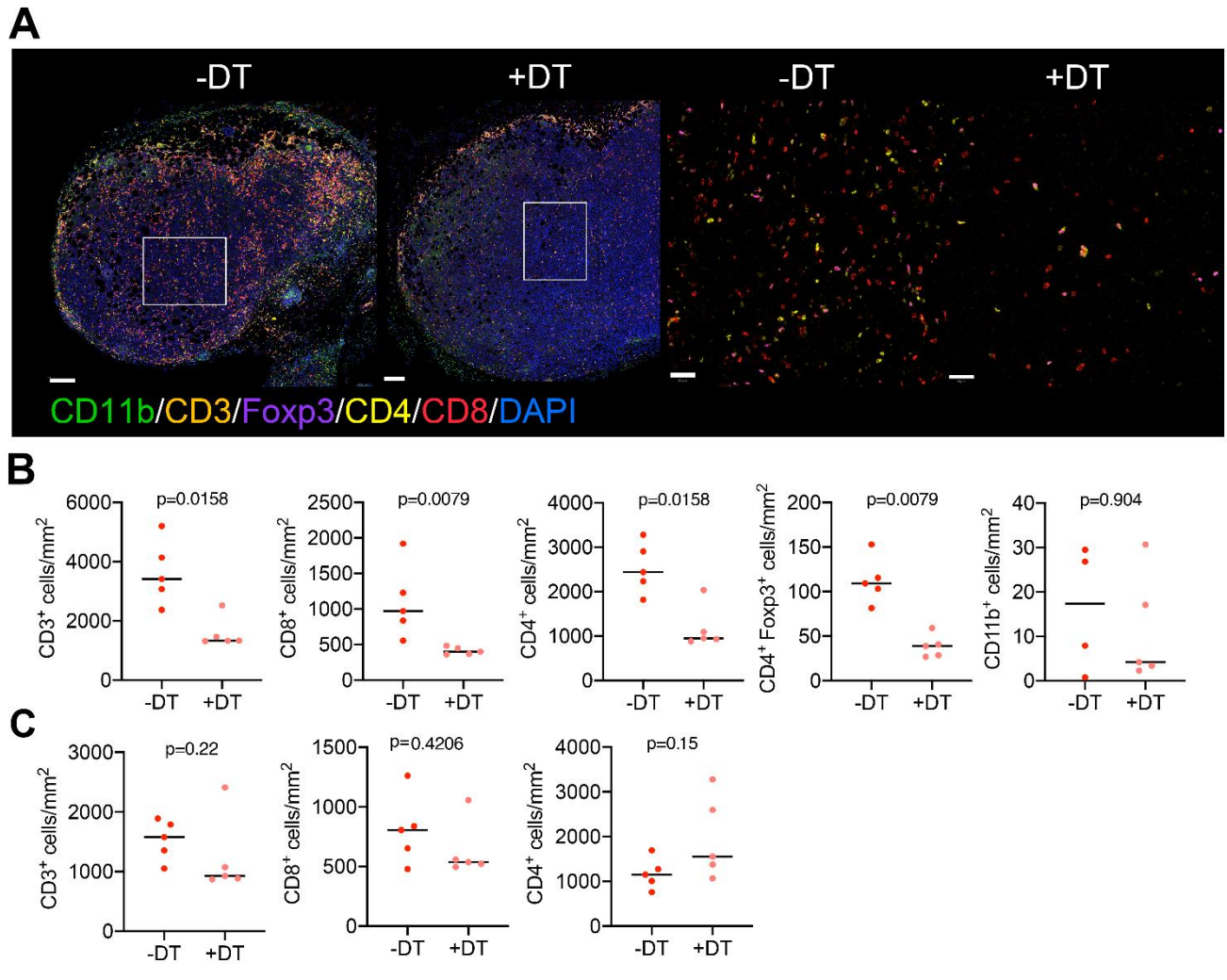
A
-DT
+DT
-DT
+DT
CD11b/CD3/Foxp3/CD4/CD8/DAPI
B
p=0.0158
p=0.0079
p=0.0158
p=0.0079
p=0.904
CD3+ cells/mm2
CD8+ cells/mm2
CD4+ cells/mm2
CD4+ Foxp3+ cells/mm2
CD11b+ cells/mm2
-DT
+DT
C
p=0.22
p=0.4206
p=0.15
CD3+ cells/mm2
CD8+ cells/mm2
CD4+ cells/mm2
-DT
+DT

Figure 5

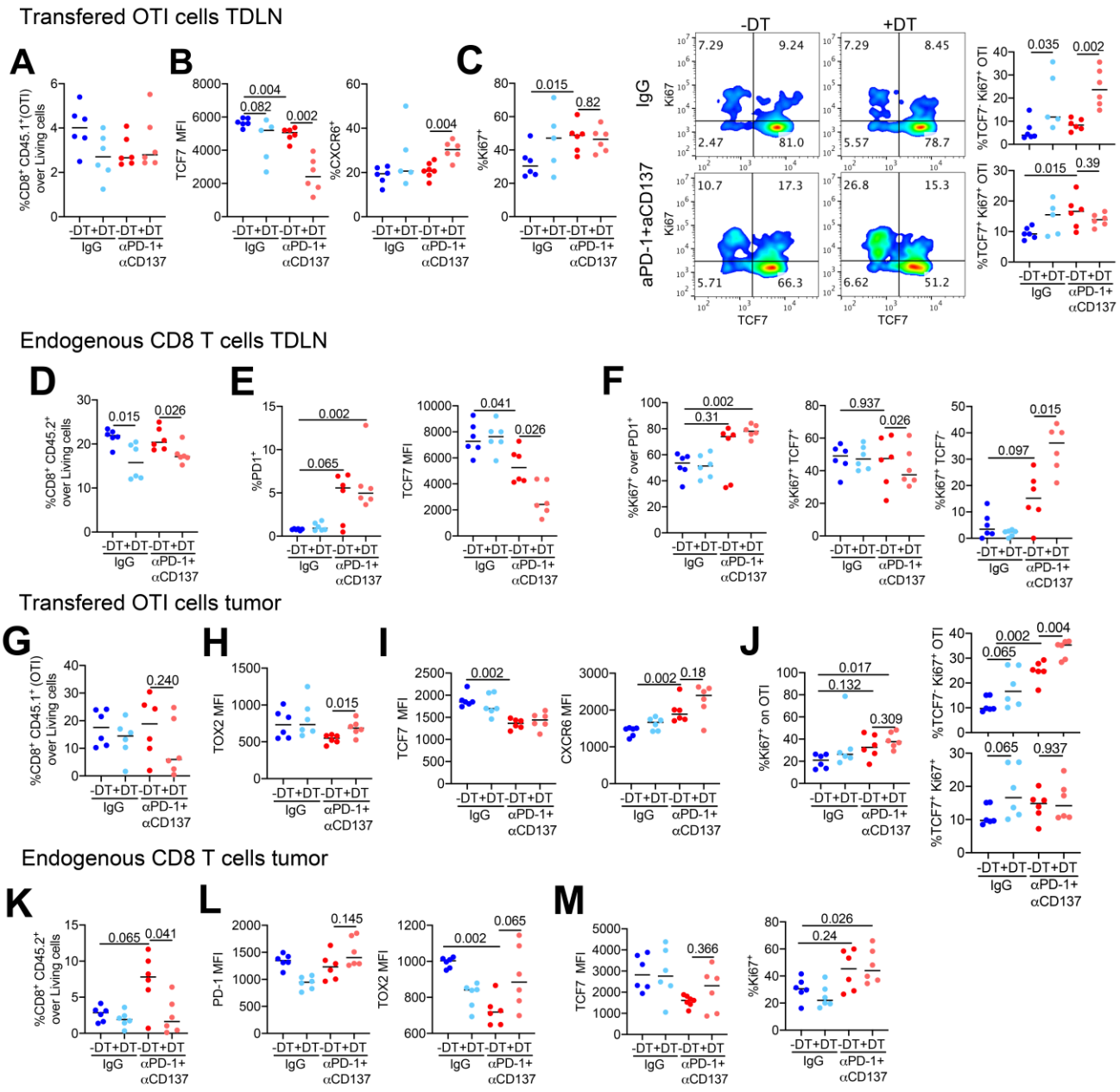
Transfered OTI cells TDLN
A
B
C
-DT
+DT
IgG
aPD-1+aCD137
Ki67
TCF7
Endogenous CD8 T cells TDLN
D
E
F
Transfered OTI cells tumor
G
H
I
J
Endogenous CD8 T cells tumor
K
L
M
-DT+DT
IgG
αPD-1+
αCD137

Figure 6

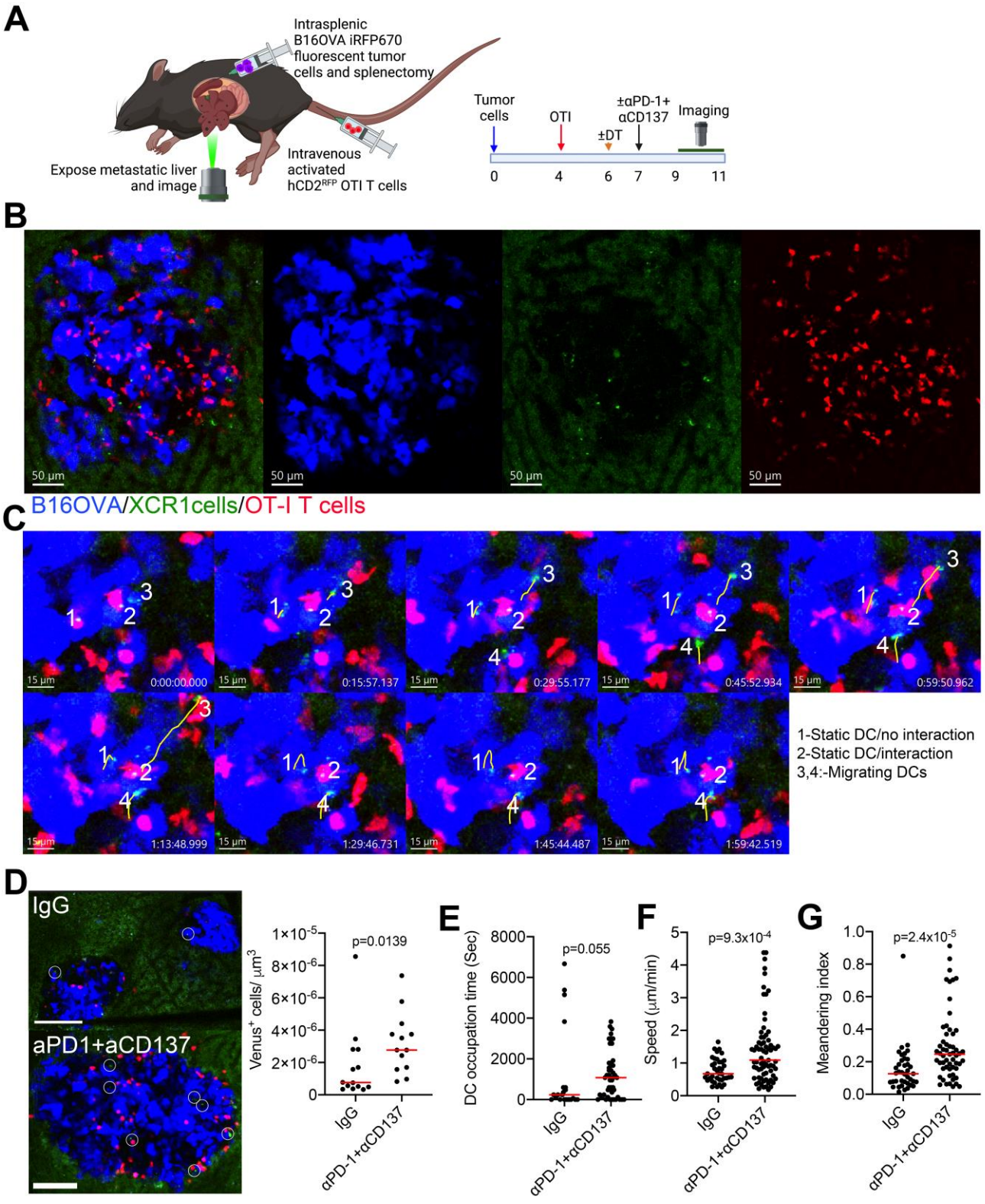
A
Intrasplenic
B16OVA iRFP670
fluorescent tumor
cells and splenectomy
Intravenous
activated
hCD2RFP OTI T cells
Expose metastatic liver
and image
Tumor
cells
OTI
±DT
±αPD-1+
αCD137
Imaging
0
4
6
7
9
11
B
50 µm
C
B16OVA/XCR1cells/OT-I T cells
15 µm
0:00:00.000
0:15:57.137
0:29:55.177
0:45:52.934
0:59:50.962
1:13:48.999
1:29:46.731
1:45:44.487
1:59:42.519
1-Static DC/no interaction
2-Static DC/interaction
3,4:-Migrating DCs
D
IgG
aPD1+aCD137
Venus+ cells/ µm3
p=0.0139
IgG
aPD-1+αCD137
E
DC occupation time (Sec)
p=0.055
F
Speed (µm/min)
p=9.3x10-4
G
Meandering index
p=2.4x10-5

Figure 7

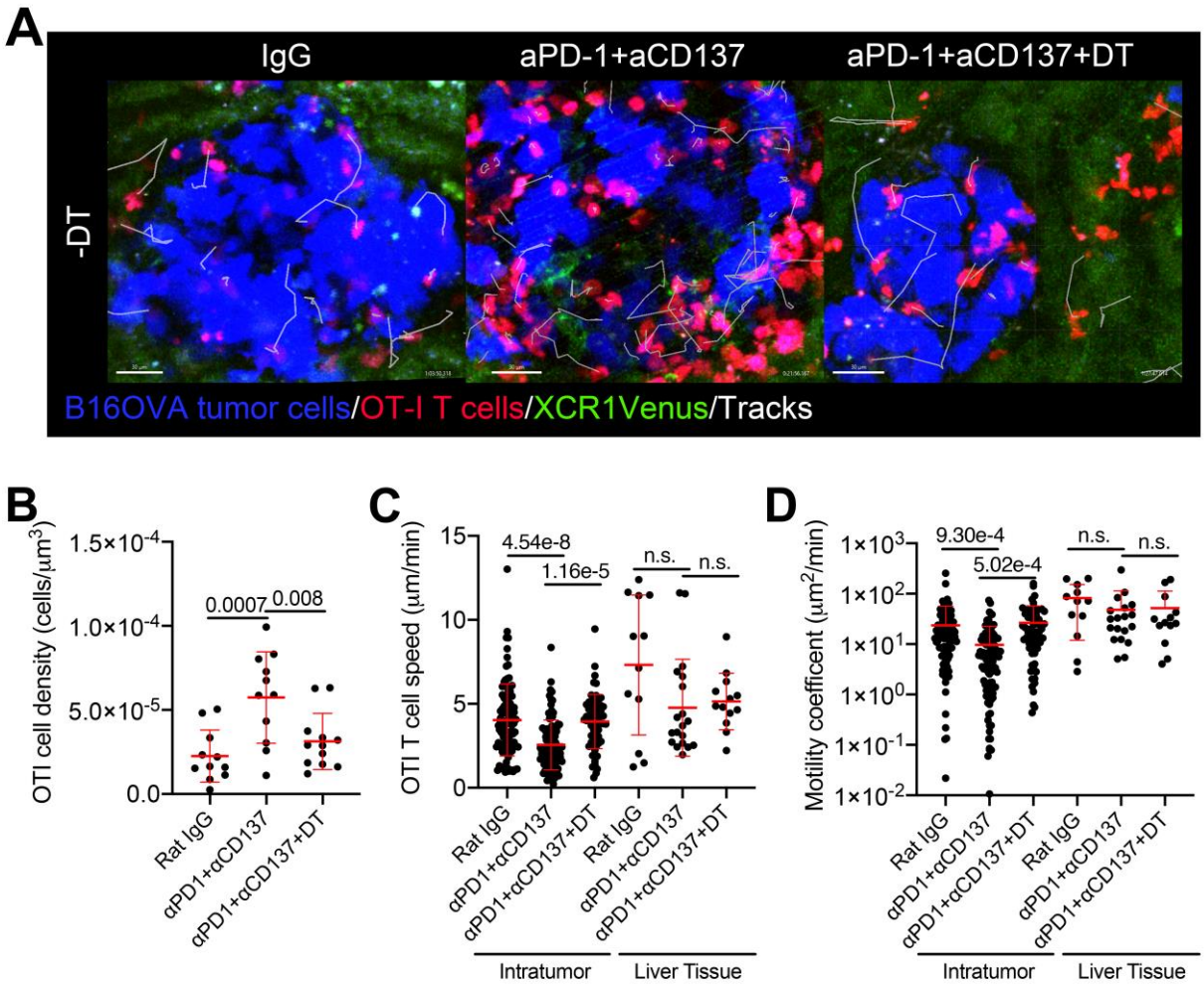
A
IgG
aPD-1+aCD137
aPD-1+aCD137+DT
-DT
B16OVA tumor cells/OT-I T cells/XCR1Venus/Tracks
B
OTI cell density (cells/μm3)
1.5×10-4
1.0×10-4
5.0×10-5
0.0
0.0007
0.008
Rat IgG
αPD1+αCD137
αPD1+αCD137+DT
C
OTI T cell speed (μm/min)
15
10
5
0
4.54e-8
1.16e-5
n.s.
n.s.
Rat IgG
αPD1+αCD137
αPD1+αCD137+DT
Intratumor
Liver Tissue
D
Motility coefficent (μm2/min)
1×103
1×102
1×101
1×100
1×10-1
1×10-2
9.30e-4
5.02e-4
n.s.
n.s.
Rat IgG
αPD1+αCD137
αPD1+αCD137+DT
Intratumor
Liver Tissue